AUT Journal of Electrical Engineering

AUT J. Elec. Eng., 53(2) (2021) 233-248
DOI: 10.22060/eej.2021.19544.5400

Fuzzy Self-tuning PI Controller for Field-weakening Control System of an Axial Flux Switching Permanent Magnet Motor

H. Radmanesh[1], . Rahmani Fard[2*]

[1]Shahid Sattari Aeronautical University of Science and Technology, Tehran, Iran.
[2]Electrical Engineering Department, Pooyesh Institute of Higher Education, Qom, Iran

ABSTRACT: In this paper, based on the vector control of axial field flux switching permanent magnet (AFFSPM) motor, an optimized field-weakening control method of AFFSPM motor is proposed. A new AFFSPM motor with 12 stator slots (S) and 19 rotor poles (P) is taken as the object to simulate and optimize the flux-weakening speed control. The AFFSPM motor adopts constant torque control with the maximum torque per ampere below the base speed, which reduces motor losses, improves the efficiency of the inverter and adopts constant power and sub-regional speed control above the rated speed. By combining the cross-axis current and direct-axis current in the flux weakening control method, the power factor of the AFFSPM motor can be improved and speed range can be extended. By considering the speed fluctuation in field weakening control, and the fuzzy self-tuning PI control method is proposed to improve the performance of the AFFSPM motor field weakening control. To verify the feasibility of proposed control method, Co-Simulation is used. Finally, the control algorithm of the drive system is implemented in a prototype of AFFSPM motor.

Review History:
Received: Jan. 23, 2021
Revised: Apr. 03, 2021
Accepted: May. 10, 2021
Available Online: Sep. 01, 2021

Keywords:
permanent magnet
Fuzzy, field-weakening
flux switching.

1- INTRODUCTION

The axial field flux switching permanent magnet (AFFSPM) motor as an efficient drive system, has been widely used in the electric vehicle industry in the recent years [1-5]. The use of rare earth magnet materials with high remanence and high coercivity, such as neodymium iron boron have greatly improved the performance of the permanent magnet synchronous motors and promoted the development of the permanent magnet synchronous motors [6]. With the advantages of high-power density, low loss, high efficiency, large torque density, low vibration and noise, AFFSPMs are highly valued by electric vehicles and become the mainstream of the most competitive electric drive systems for electric vehicles Motor [7- 9]. Due to constant limitation of the permanent magnet flux linkage, the field weakening speed regulation of permanent magnet synchronous motors is much more complicated than other motors. In addition, the AFFSPM motors for electric vehicles require constant torque output in the constant torque region, which may be stable, fast tracking of input commands, and require high control accuracy of factors such as position, torque ripple, etc., to meet the functions of starting and climbing of electric vehicles. In the constant power zone, a wide speed range is required to meet the acceleration of electric vehicles at high speeds and other functions [10]. Therefore, the drive system is required to have better dynamic response capabilities and a wider range of field-weakening speed regulation.

The improvement of the speed regulation performance of PM synchronous motor is mainly devoted to the motor structure and control method. For the motor structure, researchers have proposed various PM materials and structural improvements to promote the speed control system [9]. For the control method, the control strategy of vector control and field weakening control are proposed to improve the speed control system [10, 11].

A method based on six-step voltage is proposed in [12]. In this method, the phase angle of the motor is controlled to weaken the magnetic field and adjust the output torque of the motor.

The most widely used method in the field-weakening area was presented in [13]. It uses a voltage controller to improve the reference of i_d. Therefore, the current would not lose control. Three controllers work together in the field-weakening area. The control performance is specified by the parameters of the controllers; therefore, it is very hard to acquire the best parameters for the three controllers simultaneous. Based on single current regulator and variable q-axis voltage, a field weakening control method is presented in [14]. By full use of the DC voltage, the motor runs at the optimum operating point. Therefore, the efficiency and load capacity of the moto are improved.

An adaptive field weakening control method is presented in [15]. The important purpose is to get field weakening

*Corresponding author's email: javad.rahmani.fard@gmail.com

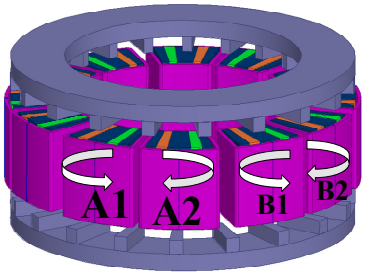

Fig. 1. Motor topology.

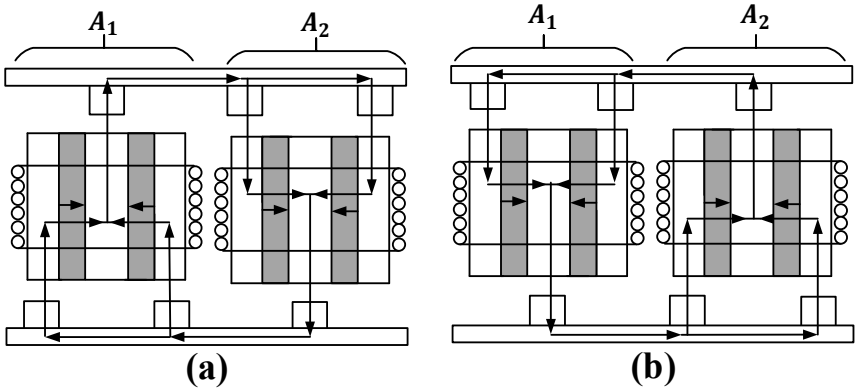

Fig. 2. Operation principles (a) Maximum positive flux linkages, (b) Maximum negative flux linkages

control by repressing the current controller from reaching saturation.

The current controller begins to saturate as soon as the inverter voltage reaches the maximum value of the DC voltage. The adaptive field weakening controller generates a demagnetizing current to warrant that the motor operates in a field-weakening area.

By transforming the q-axis voltage to single current regulator, a field weakening control method is presented in [16]. The q-axis voltage reference value of the motor can trace the output torque and the speed of the motor in real time to warrant that the motor runs stably.

This article takes the axial field flux switching permanent magnet (AFFSPM) motor as the object, and combines the field weakening control and fuzzy self-tuning PI control to further improve the speed regulation performance and stability of the motor.

2- THE AFFSPM MOTOR CONTROL PRINCIPLE

2.1) Configuration and operation principle

Figures 1 and 2 show the configuration and operation principle of the 12Slots/19Poles YASA-AFFSSPM machine. The design and the operation principle are proposed with details in [11].

2.2) 3-D FEM model

The equations solved in the 3D-FEM are as follows

$$B = \nabla \times \psi \tag{1}$$

$$\nabla \times \frac{1}{\mu} B = \begin{cases} 0 \text{ (air and cores)} \\ \nabla \times H_c \text{(PMs)} \\ J_s \text{ (coils)} \end{cases} \tag{2}$$

$$\nabla \times J_s = -\sigma \frac{dB}{dt} \tag{3}$$

where B and ψ are magnetic flux density and magnetic vector potential. μ and σ are magnetic permeability and electrical conductivity. J_s and H_c are current density and coercive field strength. The 3-D FEM model of the 12S/19P YASA-AFFSSPM motor is provided in the "Ansys Maxwell 16" software. The 3D mesh of the 12S/19P YASA-AFFSSPM motor is illustrated in Fig. 3.

The open-circuit magnetic flux density distribution is shown in Fig. 4.

Fig. 5 shows the three-phase self-inductances and mutual inductances of a 12/19 YASA-AFFSSPM motor obtained by finite element simulation. The inductance changes twice in the electric cycle but the amplitude changes are small.

Fig.6 shows the calculated d and q axes inductances. It can be seen that the difference between L_d and L_q is minor, and L_q / L_d is about 1.13. Therefore, the 12/19 YASA-AFFSSPM motor has a salient pole effect $\left(L_d \neq L_q\right)$. Furthermore, the saliency can be tracked to perform sensorless control of the high-frequency injection method.

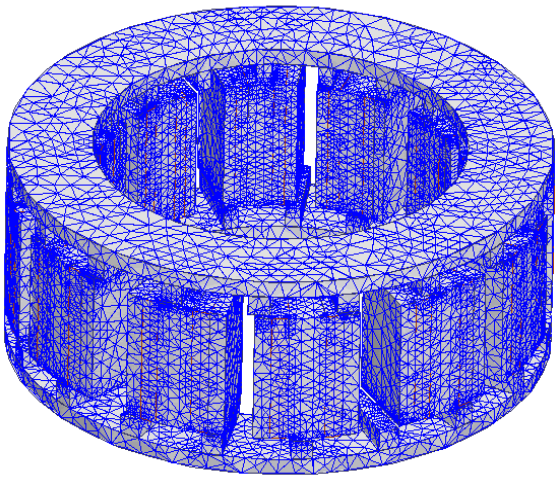

Fig. 3. 3-D mesh of the 12S/19P YASA-AFFSSPM motor.

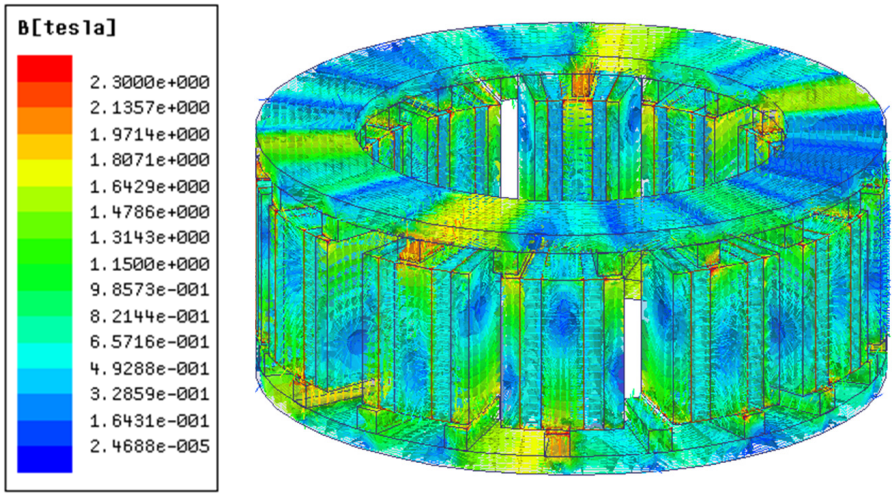

Fig. 4. Open-circuit field distribution

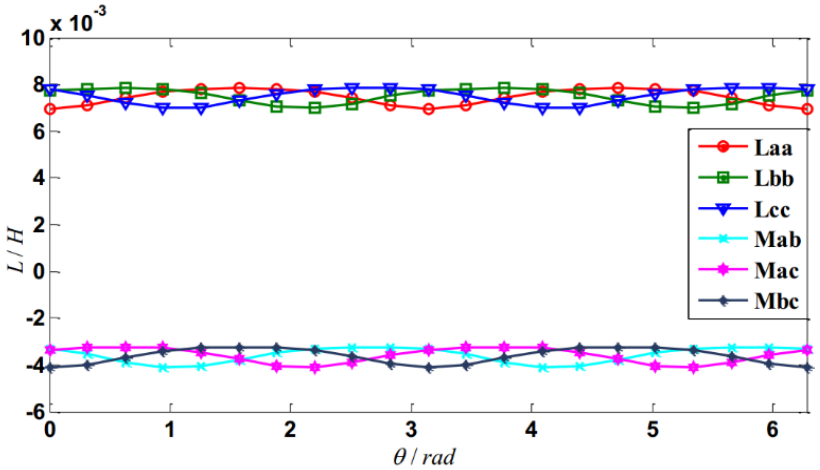

Fig. 5. Three-phase self-inductances and mutual inductances

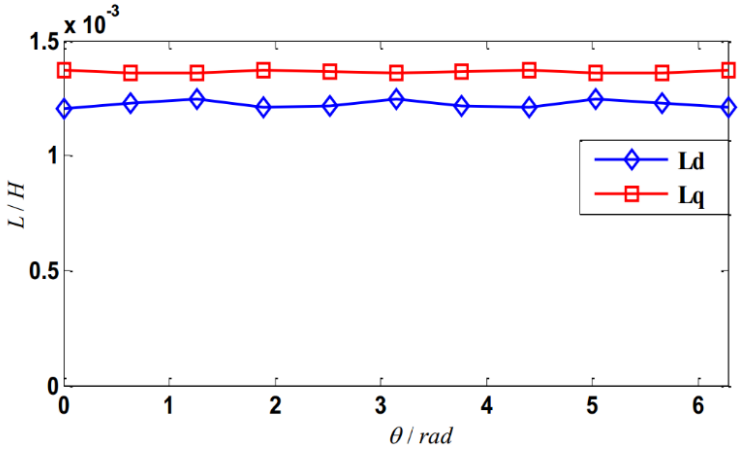

Fig.6. d/q axes inductances

2.3) Mathematical Model of AFFSPM Motor

Using the traditional permanent magnet synchronous motor (PMSM) modeling analysis method, the mathematical model of the AFFSPM motor in the d-q coordinate system is obtained. The basic equation is as follows:

$$\begin{cases} \psi_d = L_d i_d + \psi_f \\ \psi_q = L_q i_q \end{cases} \tag{4}$$

The voltage equations are as follows

$$\begin{cases} u_d = L_d \dfrac{di_d}{dt} - \omega_r L_q i_q + R_s i_d \\ u_q = L_q \dfrac{di_q}{dt} + \omega_r \left(L_d i_d + \psi_f \right) + R_s i_q \end{cases} \tag{5}$$

The electromagnetic torque and motion equations can express as

$$\begin{cases} T_e = \dfrac{3}{2} p \psi_f i_q + \dfrac{3}{2} p \left(L_q - L_d \right) i_d i_q \\ T_e - T_l = \dfrac{J}{p} \dfrac{d\omega_r}{dt} + B\omega_r \end{cases} \tag{6}$$

In the equations, R_s and R_f are stator resistance and field winding resistance. L_d and L_q are the d-q axes armature inductances. i_d, i_q are d-q axes armature current. u_d and u_q are d-q axes armature voltage. ψ_d, ψ_q, ψ_f are d-q axes flux linkage, the permanent magnet flux linkage. T_l is load torque, ω_r is the mechanical angular velocity, p is the number of pole pairs, J is the moment of inertia and B is the coefficient of friction.

2.4) Voltage Limit Ellipse and Current Limit Circle

The maximum voltage provided by the inverter to the AFFSPM motor is affected by the DC side voltage and the conversion efficiency of the inverter, and meets certain constraints.

For stator voltage $u_s = \sqrt{u_d^2 + u_q^2}$

Combined with the mathematical model of the AFFSPM motor, we have:

$$\left(L_d i_q + \psi_f \right)^2 + \left(L_q i_q \right)^2 \le \left(\frac{u_{s\max}}{\omega_r} \right)^2 \tag{7}$$

where, $u_{s\max}$ is the allowable limit value of u_s.

Similarly, the output of the current capacity of the inverter is also limited by its capacity, and the motor stator current also has a limit value. which follows:

$$i_d^2 + i_q^2 \le i_{s\max}^2 \tag{8}$$

Where, $i_{s\max}$ is the maximum stator current, generally set $i_{s\max}$ equal to the rated value. Equations (3) and (4) constitute the voltage limit ellipse and the current limit circle, as shown in the Fig. 7 [17, 18].

Since i_s has to satisfy both the current limit and the voltage limit equation, the stator current vector must fall within the common range of the voltage limit ellipse and the current limit circle.

2.5) Maximum Torque Current Ratio

When running in the constant torque state, any point on the constant torque curve corresponds to a pair of i_d and i_q for the AFFSPM motor. The stator current vector formed by each pair of i_d and i_q can produce the same magnitude of electromagnetic torque, and there is a stator current vector with the smallest amplitude. Connecting points that meet this condition, the corresponding curve is called the Maximum Torque per Ampere (MTPA) curve [18]. According to the mathematical model of AFFSPM motor

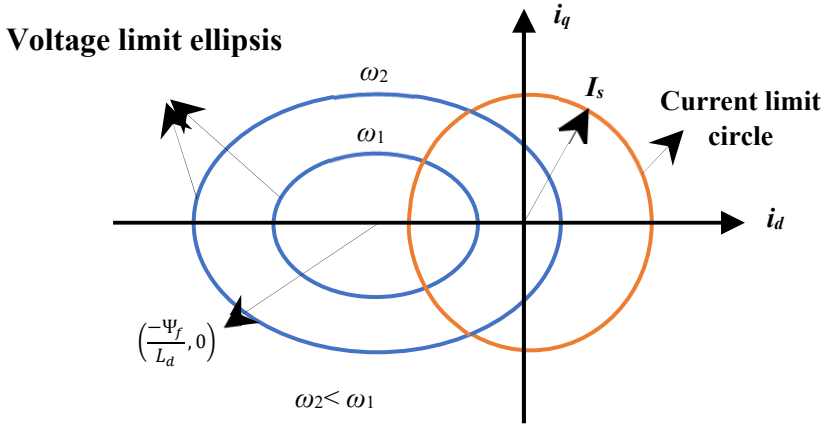

Fig. 7. Voltage limit ellipse and current limit circle

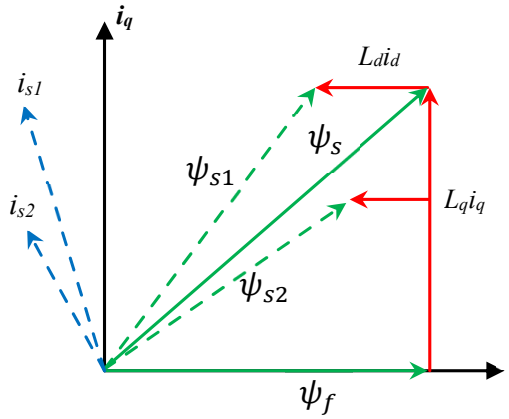

Fig. 8. Vector diagram of field weakening control mode

$$\begin{cases} I_s = \sqrt{i_d^2 + i_q^2} \\ T_e = \dfrac{3}{2} p \left(\psi_f + \dfrac{3}{2} p \left(L_q - L_d \right) i_d \right) i_q \end{cases} \tag{9}$$

The auxiliary function is defined as:

$$G = \sqrt{i_d^2 + i_q^2} - \lambda \left\{ T_e - \frac{3}{2} p \left(\psi_f + \frac{3}{2} p \left(L_q - L_d \right) i_d \right) i_q \right\} \tag{10}$$

Therefore, there is the equation satisfied by the i_d and i_q currents with the smallest amplitude under the same electromagnetic torque in the case of the maximum torque per Ampere, which follows as

$$i_d = \frac{-\psi_f + \sqrt{\psi_f^2 + 4\left(L_d - L_q \right) i_q^2}}{2\left(L_d - L_q \right)} \tag{11}$$

When the AFFSPM motor is running at a constant torque on the MTPA curve, the stator current amplitude is the smallest, which is beneficial in reducing the copper loss in the motor operation, improving the efficiency of the inverter, and reducing the energy loss.

3- FIELD WEAKENING CONTROL STRATEGY

For AFFSPM, compared to a motor with an electrically excited rotor, the rotor magnetic field cannot be directly weakened. Field weakening is usually performed by adjusting the amplitude and phase angle of the stator current. Essentially, it increases the i_d of the direct-axis demagnetization current component of the motor, to counteract the magnetic field generated by the permanent magnet. Thereby, weakening the air gap magnetic field of the motor to equivalently directly weaken the excitation magnetic field to achieve the purpose of field weakening control or by reducing the quadrature axis demagnetization current component i_q to weaken the magnetic field [14]. The combination of the two methods, which have better magnetic weakening effect, can be seen in Fig. 8.

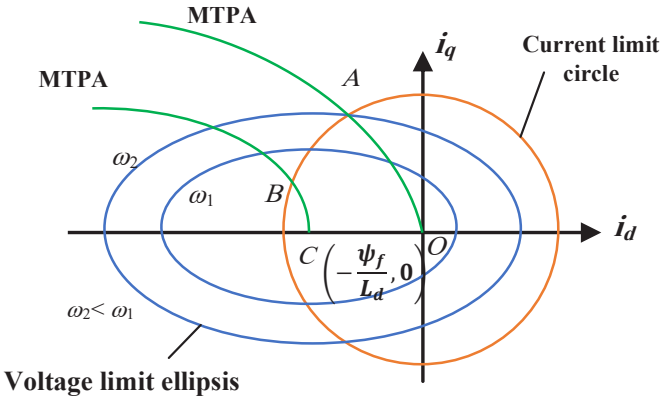

Fig. 9. Field weakening control trajectory

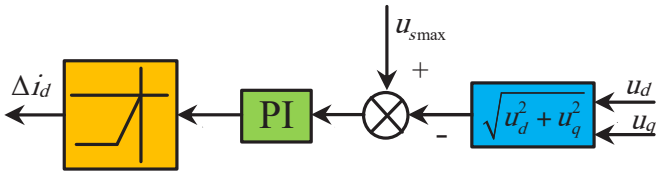

Fig. 10. Negative current compensation control based on i_d

There are many field weakening control methods, and the field weakening methods used for different permanent magnet synchronous motors are also different. In this paper, the current regulator method is used for field weakening control, and the stator quadrature axis current is modulated by the difference between the actual value of the motor angular frequency and the given value, and the stator direct axis current is determined by the maximum torque current ratio scheme. On the basis of the original double closed-loop structure, one more field weakening loop is added, and the difference between the given voltage and the DC terminal voltage is used as the adjustment to control the demagnetization current setting, and the deep field weakening control is performed by controlling the direct axis demagnetization current. During the operation, the constant torque area is controlled to switch to the field weakening area by comparing the real-time voltage of the stator and the maximum voltage of the inverter.

The specific control process can be divided into three areas:

According to MTPA control at different speeds, in the constant torque area and on the curve of maximum torque to current ratio, any point of the OA curve (as shown in Fig. 9) is constant torque. In the field weakening zone I, when the AC output side voltage of the inverter reaches its maximum value, it will cause the saturation of the current inner loop regulator. By increasing the demagnetization current component of the direct axis, the stator current trajectory of the motor can run along AB, and the motor speed will increase accordingly. The control method is as follows

$$\begin{cases} \sqrt{u_d^2+u_q^2} \le u_{s\max} & \Delta i_d = 0 \\ \sqrt{u_d^2+u_q^2} > u_{s\max} & \Delta i_d < 0 \end{cases} \tag{12}$$

The specific implementation is shown in Fig. 10.

In zone II field weakening, when the motor reaches the position corresponding to the coordinate of point C, the quadrature axis current component can be continuously adjusted to perform field weakening.

4- FUZZY SELF-TUNING PI

The traditional PI control is greatly affected by uncertain factors such as motor parameter changes and load disturbances, and the PI parameters are fixed, and also the anti-interference ability is poor, resulting in a decrease in control quality. Therefore, the high-performance fuzzy adaptive PI control of control theory is adopted to improve the control performance of the system [15]. Fuzzy self-tuning PI uses fuzzy inference to adjust PI parameters online. By judging the speed deviation value and the rate change of the input speed deviation value, the fuzzy control rules are used to set K_p and K_i of the PI regulator online, so that the control system does not sacrifice the fast response. Under the premise of ability and dynamic tracking performance, it has a high anti-disturbance ability and certain adaptive ability.

Fig. 11. e, ec, ΔK_p and ΔK_i membership function

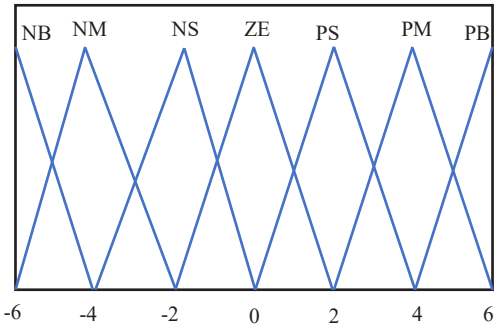

Table 1. Rules of ΔK_p

e	ec						
	NB	NM	NS	ZE	PS	PM	PB
NB	PB	PB	PM	PM	PS	ZE	ZE
NM	PB	PB	PM	PS	PS	ZE	NS
NS	PM	PM	PM	PS	ZE	NS	NM
ZE	PM	PM	PS	ZE	NS	NM	NM
PS	PS	PS	ZE	NS	NS	NM	NM
PM	*PS*	*ZE*	*NS*	*NM*	*NM*	*NM*	*NB*
PB	*ZE*	*ZE*	*NM*	*NM*	*NM*	*NB*	*NB*

Table 2. Rules of ΔK_i

e	ec						
	NB	*NM*	*NS*	*ZE*	*PS*	*PM*	*PB*
NB	*NB*	*NB*	*NM*	*NM*	*NS*	*ZE*	*ZE*
NM	*NB*	*NB*	*NM*	*NS*	*NS*	*ZE*	*NS*
NS	*NB*	*NM*	*NS*	*NS*	*ZE*	*PS*	*PS*
ZE	*NM*	*NM*	*NS*	*ZE*	*PS*	*PM*	*PM*
PS	*NM*	*NS*	*ZE*	*PS*	*PS*	*PB*	*PB*
PM	*ZE*	*ZE*	*PS*	*PS*	*PM*	*PB*	*PB*
PB	*ZE*	*ZE*	*PS*	*PM*	*PM*	*PB*	*PB*

Denote the speed deviation by e, deviation change rate by $ec(k)$ and PI parameter adjustment by ΔK_p, ΔK_i. Each ΔK_p, ΔK_i contains 7 fuzzy subsets {NB (negative large), NM (negative medium), NS (negative small), ZE (Zero), PS (Positive Small), PM (Positive Middle), PB (Positive Large)}, and the continuity domain is [-6, 6].

The fuzzy PI parameter calculation follows as

$$\begin{cases} K_p = K_{po} + \Delta K_p \\ K_i = K_{io} + \Delta K_i \end{cases} \tag{13}$$

Now the introduced quantitative factors K_e and K_{ec}, e is multiplied by the quantization factor K_e, and ec is multiplied by K_{ec} and input into the two-dimensional fuzzy controller. Output PI Controller increment ΔK_p and ΔK_i are used to adjust the original values of K_{po} and K_{io} of the PI controller. For the convenience of calculation, e, ec, ΔK_p and ΔK_i all adopt triangular membership function [15], as shown in the Fig. 11.

The control rule tables of PI parameter adjustment ΔK_p and ΔK_i are shown in Table1 and Table2.

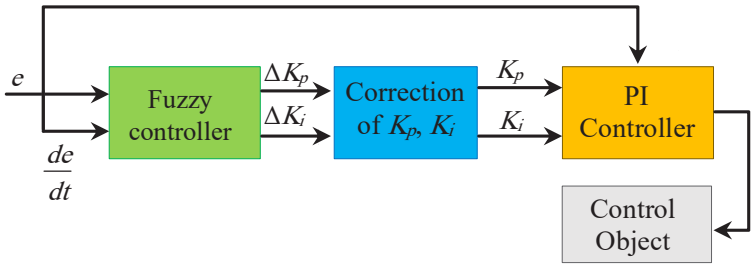

Fig. 12. Block diagram of fuzzy control principle

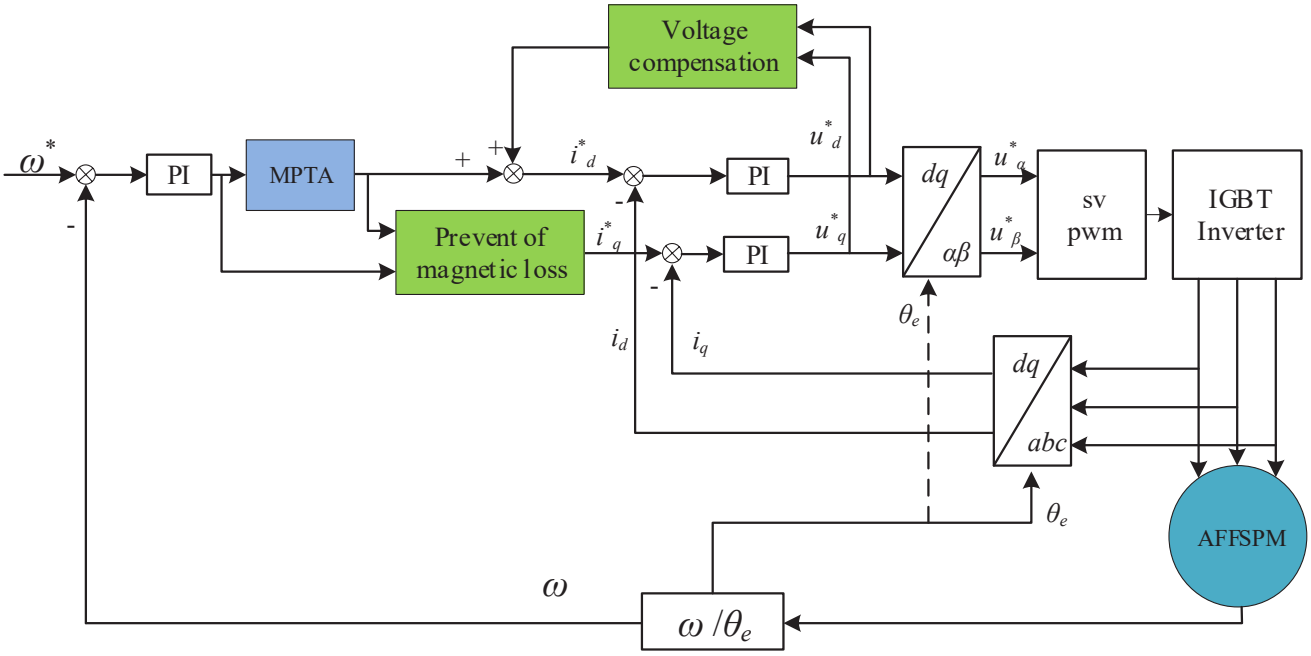

Fig. 13. Control block diagram of three-phase AFFSPM motorwaveform

The 49 inference sentences in the following form are inputted into the Mamdani fuzzy controller.

If (e is NB) and (ec is NB) then K_p is PB and K_i is NB

In operation, different inputs will result in different fuzzy outputs. However, these inference sentences correspond to the fuzzy output of ΔK_p and ΔK_i, which cannot directly control the system and must be defuzzified. By using the center of gravity method for defuzzification, the real precise value of ΔK_p and ΔK_i are obtained, and the PI parameter self-tuning are realized. The fuzzy control process is shown in Fig.12.

The overall control block diagram of the system is shown in Fig. 13.

Table 3: Parameters of 12S/19P YASA- AFFSSPM motor

Parameter	**Value**
Rated speed n / rpm	200
Rated Torque T_n / N.m	12
Rated Power P / kW	0.75
PM flux linkage φ_m / Wb	0.10
Stator resistance R / Ω	0.65
dq axes rated current I_d=I_q /A	10
Sampling time T / s	10^{-4}

Table: 4. comparison between two fuzzy PI control

Items	Traditional fuzzy PI control	new fuzzy PI control
The ratio of overshoot	6%	0%
settling time	2.5s	2.3s
torque ripple	37%	18%

5- CO-SIMULATION RESULTS AND ANALYSIS

In this study, we use Co-Simulation to investigate the performance of the proposed method. Certainly, a simple linear model is not sufficient for a precise analysis. If the magnetic saturation and time/space harmonics and other factors have been considered, the motor model will be nonlinear and the analysis will be much closer to reality. In this study, we provide the 3-D FEM model of the proposed motor in the "ANSYS MAXWELL" software. Then, in order to create the electrical and electromechanical parts of drive system, the "ANSYS SIMPLORER" software is employed. Finally, the control algorithm of the drive system is implemented in "Simulink/MATLAB". circuit and control system at the same time. ANSYS MAXWELL and ANSYS SIMPLORER are coupled in the same environment, ANSYS Workbench. For linking Simplorer to Simulink/MATLAB, a compiler running in Matlab is needed. Ansys Path in MATLAB must be set. In Matlab, we created our model with an s-function called "AnsoftSFunction". In the link assignment area, we add as many Inputs and Outputs we need. Now go to Simplorer and create Simulink Subcircuit. The Co-Simulation lets us analysis of the motor with 3-D finite element method, external drive.

The motor parameters are shown in Table 3.

The constant power field weakening zone speed is between 200 rpm and 500 rpm. Now take 400 rpm, torque reference changes from 18Nm and 5Nm and then to 2.5Nm., and the simulation result of field weakening speed regulation under traditional PI control is shown in the Fig 14.

Moreover, with the proposed fuzzy PI control, the simulated waveforms are shown in Fig. 15.

It can be seen from the simulation results that the constant torque, transitions to constant power before 0.05s, and the field weakening speed regulation can track the given speed.

By comparing the simulation waveforms in (a) in Fig. 14 with (a) in Fig. 15, it can be concluded that by using traditional fuzzy PI control, the ratio of overshoot is greater than that of the new fuzzy PI control, and has many vibrations. Moreover, the speed is stable at 2.5s, while in the new fuzzy PI control, the speed is almost stable at 2.3s.

A comparison between the simulation waveforms in (b) and (c) in Fig. 14 with (b) and (c) in Fig. 15 shows that the current/torque ripple of the new fuzzy PI control is smaller than the current/torque ripple of the traditional fuzzy PI control. For better comparison, the results are listed in table 4.

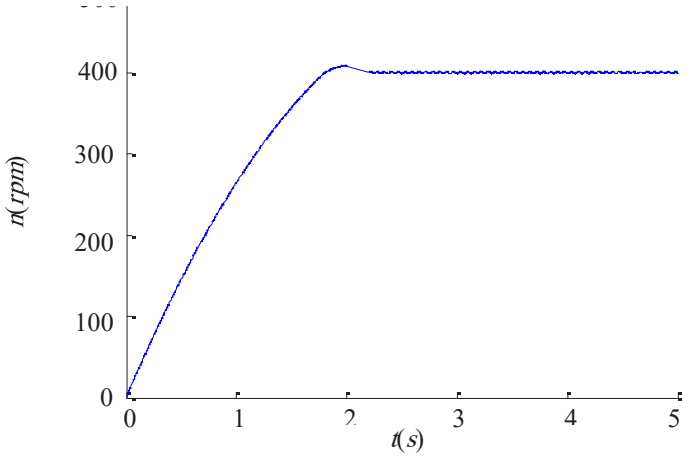

(a)

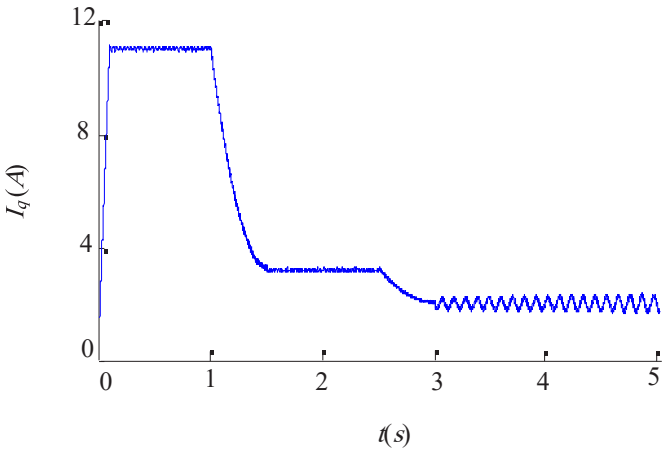

(b)

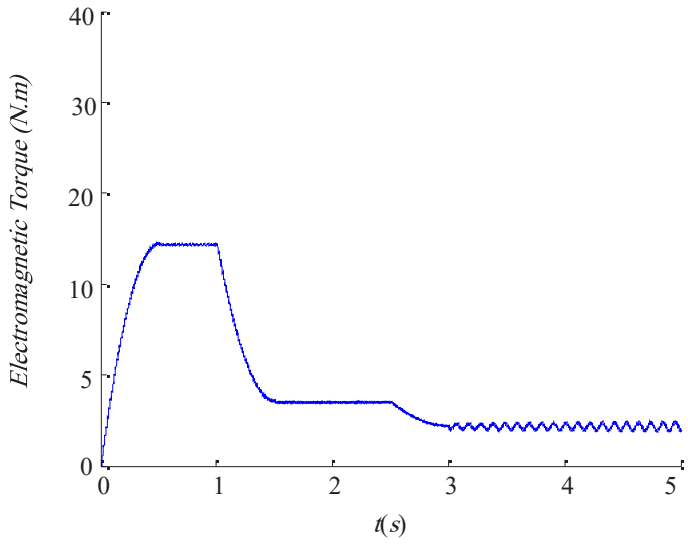

(c)

Fig. 14. Simulation result under traditional PI control (a) The speed waveform (b) The id current waveform (c) The electromagnetic torque waveform

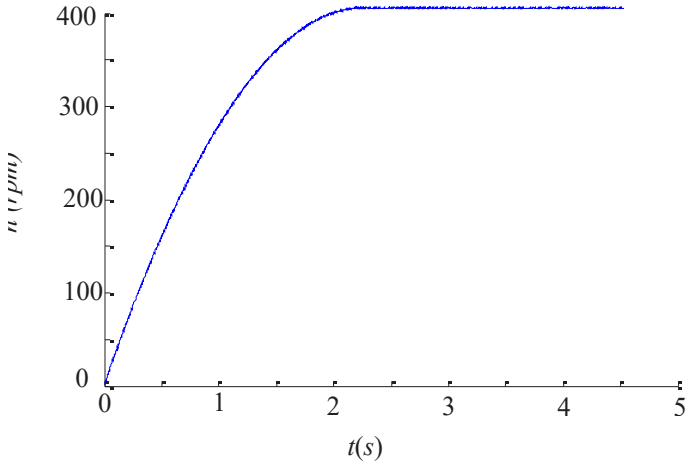

(a)

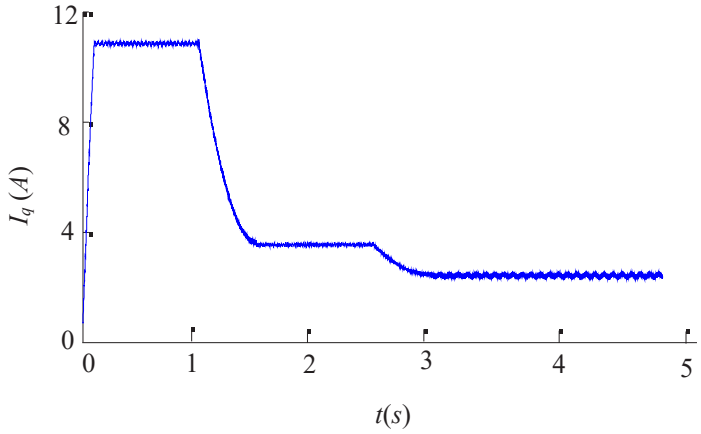

(b)

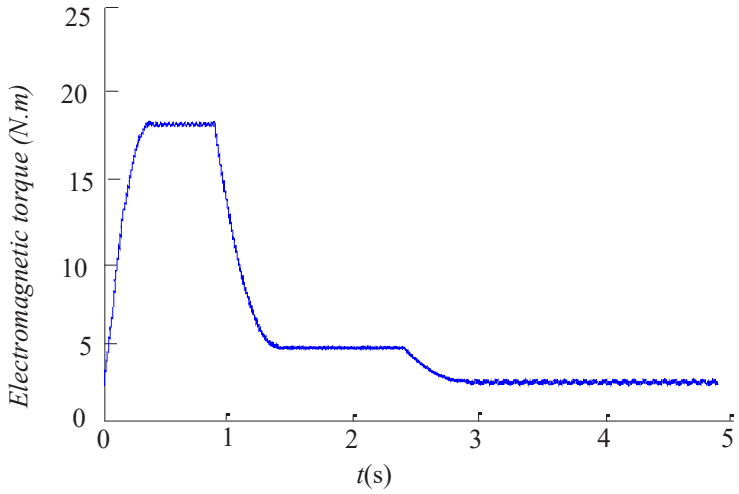

(c)

Fig. 15. Simulation result under proposed fuzzy PI control (a) The speed waveform (b) The id current waveform, (c) The electromagnetic torque waveform

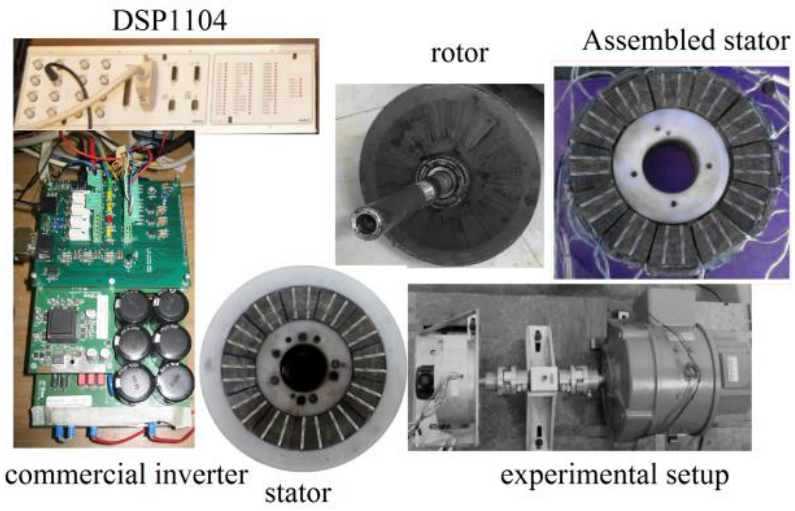

Fig. 16. Prototype machine and the experimental setup.

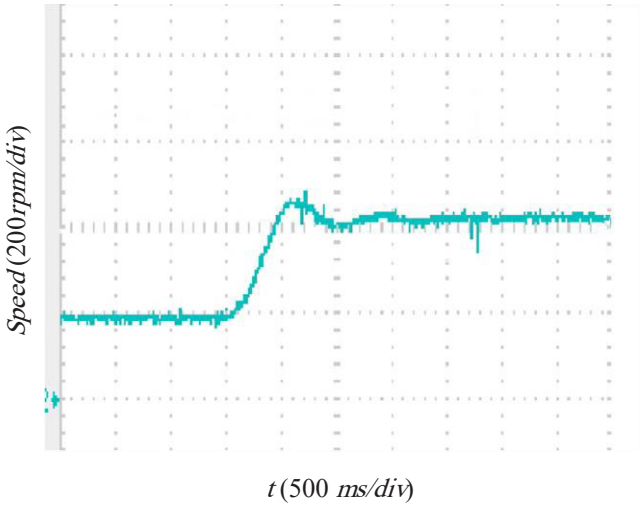

Fig. 17. Speed in conventional fuzzy-PI controller.

6- EXPERIMENTAL RESULTS

Fig. 16 depicts the prototype of the 12S/19P YASA-AFFSSPM machine and the experimental setup. The DSP1104 is the core of the digital control system. The emulate load is a 1.5 hp separately excited DC machine. At first, the load torque is 8 N.m. In the conventional and proposed fuzzy-PI control, the experimental results are shown in this section.

6.1) performance during speed changes

The reference speed suddenly changes from 200 rpm to 400 rpm, but the load torque is constant. As can be seen in Fig.s 17 and 18, in conventional fuzzy-PI controller, the speed will be stable in about 140 ms while it will be stable in about 100 ms in proposed fuzzy-PI controller.

Moreover, a comparison between Fig.17 and Fig.18 shows that the overshoot ratio and torque ripple in the new fuzzy-PI controller are smaller than those in the conventional fuzzy-PI controller. Fig.19 shows the electromagnetic torque in conventional fuzzy-PI controller and proposed fuzzy-PI controller.

6.2) Performance During Torque Changing

In order to investigate the dynamic response performance of the proposed method, the torque suddenly is enhanced. The initial value of the torque reference is 8 N.m, Then the sudden change of the load torque occurs, which is 12 N.m. The results of q-axis current response and torque response are shown in Figures. 19 and 20.

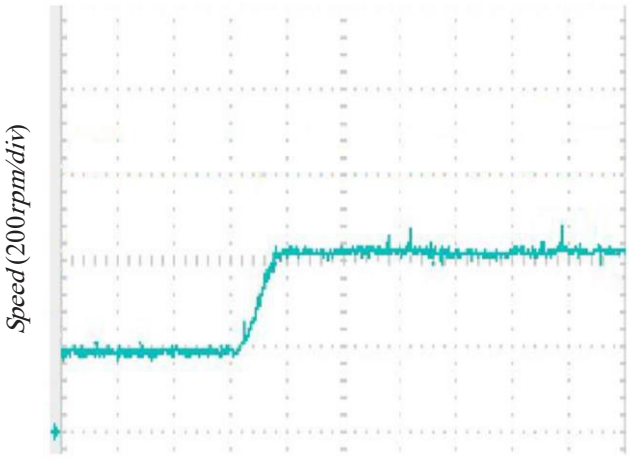

Fig. 18. Speed in proposed fuzzy-PI controller.

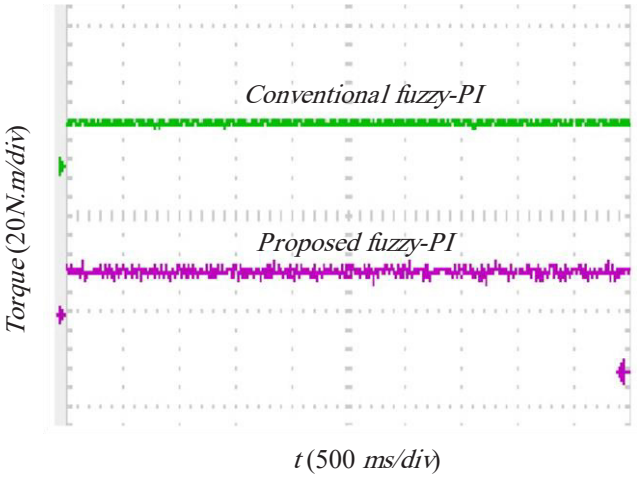

Fig. 19. Torque during suddenly changes.

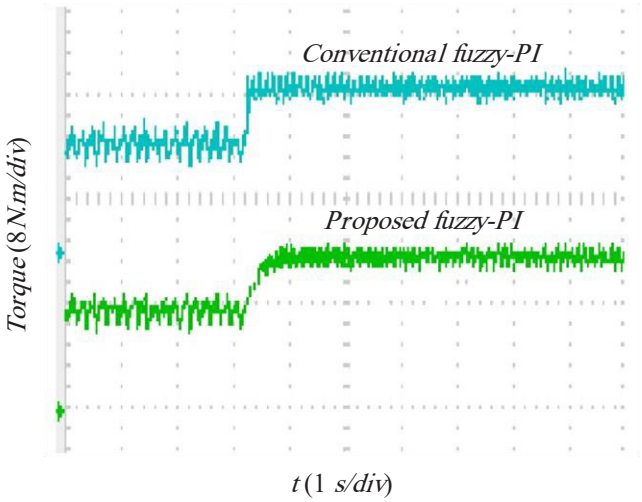

Fig. 20. I_q during suddenly changes.

7- CONCLUSION

This paper analyzes the speed regulation principle of the axial field flux switching permanent magnet (AFFSPM) motor and points out the constant torque and constant power sub-regional speed regulation in the motor speed regulation. It is proposed that using maximum torque current below the rated speed can improve the torque utilization rate of the motor and the field weakening control above the rated speed can increase the speed regulation range. In view of the torque fluctuation problem of traditional PI control, fuzzy adaptive PI is proposed to optimize the field weakening control, which is verified by simulation and experiments. It can be seen from the simulation and experiments results that the fuzzy adaptive PI improves the speed regulation performance of the permanent magnet motor in the field weakening mode.

REFERENCES

[1] Zhao, Jilong, et al. "Design of a Novel Axial Flux Rotor Consequent-Pole Permanent Magnet Machine." IEEE Transactions on Applied Superconductivity 30.4 (2020): 1-6.

[2] J. H. Kim, Y. Li, B. Sarlioglu, "Novel six-slot four-pole axial switched flux permanent magnet machine for electric vehicle," IEEE Trans. Transport. Electrific., vol. 3, no. 1, pp. 108-117, Mar. 2017.

[3] Syed, Qurban Ali Shah, Haris Kurtović, and Ingo Hahn. "New single-phase flux switching axial flux permanent magnet motor." IEEE Transactions on Magnetics 53, no. 11 (2017): 1-5.

[4] Zhang, Wei, Xingyan Liang, and Feng Yu. "Fault-tolerant control of hybrid excitation axial field flux-switching permanent magnet machines." IEEE Transactions on Magnetics 54, no. 11 (2018): 1-5.

[5] Zhao, Wenliang, Thomas A. Lipo, and Byung-Il Kwon. "A novel dual-rotor, axial field, fault-tolerant flux-switching permanent magnet machine with high-torque performance." IEEE Transactions on Magnetics 51, no. 11 (2015): 1-4.

[6] Deng, Tao, Zhenhua Su, Junying Li, Peng Tang, Xing Chen, and Ping Liu. "Advanced angle field weakening control strategy of permanent magnet synchronous motor." IEEE Transactions on Vehicular Technology 68, no. 4 (2019): 3424-3435.

[7] Zou, Yu, and Ka Wai Eric Cheng. "A Vertical Flux-Switching Permanent Magnet Based Oscillating Wave Power Generator with Energy Storage." Energies 10, no. 7 (2017): 887.

[8] Ullah, Noman, Muhammad Kashif Khan, Faisal Khan, Abdul Basit, Wasiq Ullah, Tanvir Ahmad, and Naseer Ahmad. "Comparison of Analytical Methodologies for Analysis of Single Sided Linear Permanent Magnet Flux Switching Machine: No-Load Operation." Applied Computational Electromagnetics Society Journal 33, no. 8 (2018).

[9] Zhang, Bangfu, Ming Cheng, Mingli Zhang, Wei Wang, and Yunlei Jiang. "Comparison of modular linear flux-switching permanent magnet motors with different mover and stator pole pitch." In 2017 20th International Conference on Electrical Machines and Systems (ICEMS), pp. 1-5. IEEE, 2017.

[10] Ekanayake, Sithumini, Rukmi Dutta, M. Faz Rahman, and Dan Xiao. "Direct torque and flux control of interior permanent magnet synchronous machine in deep flux-weakening region." IET Electric Power Applications 12, no. 1 (2017): 98-105.

[11] Fard, Javad Rahmani, and Mohammad Ardebili. "Design and control of a novel yokeless axial flux-switching permanent-magnet motor." IEEE Transactions on Energy Conversion 34, no. 2 (2018): 631-642.

[12] Yong-Cheol Kwon, Sungmin Kim, Seung-Ki Sul, Six-Step Operation of PMSM with Instantaneous Current control[J], IEEE Trans. On Industry Applications, 2013, Vol. 50,pp. 863-874.

[13] Kim Jang-Mok, and Sul Seung-Ki, "Speed control of interior permanent magnet synchronous motor drive for the flux weakening operation," Industry Applications, IEEE Transactions on, vol. 33, no. 1, pp. 43-48, 1997.

[14] Taiyuan Hu, Fei Lin, Kezhen Lin, etc, Flux-weakening Control of PMSM Based on Single Current Regulator and Variable Q-axis Voltage, The 15th Internation Conference on Electrical Machines and Systems (ICEMS2012), Sapporo, Japan, 2012, pp. 20-25

[15] Shi, J-L., T-H. Liu, and S-H. Yang. "Nonlinear-controller design for an interior-permanent-magnet synchronous motor including field-weakening operation." IET Electric Power Applications 1, no. 1 (2007): 119-126.

[16] Chen, Kunhua, Yukun Sun, and Bo Liu. "Interior permanent magnet synchronous motor linear field-weakening control." IEEE Transactions on Energy Conversion 31, no. 1 (2015): 159-164.

[17] Renu, K., N. Krishna Kumari, and D. S. G. Krishna. "Sensorless control of permanent magnet synchronous motor with flux weakening operation for washing machine application." In 2018 IEEE international conference on power electronics, drives and energy systems (PEDES), pp. 1-6. IEEE, 2018.

[18] Tian, Bing, Galina Mirzaeva, Qun-Tao An, Li Sun, and Dmitry Semenov. "Fault-tolerant control of a five-phase permanent magnet synchronous motor for industry applications." IEEE Transactions on Industry Applications 54, no. 4 (2018): 3943-3952.

[19] Xinhai, Jin, Zeng Yanneng, and Xu Dianguo. "Novel PMSM field-weakening control method." In IECON 2017-43rd Annual Conference of the IEEE Industrial Electronics Society, pp. 3744-3748. IEEE, 2017.

[20] Xu, Erwei, Shuhong Wang, Xu Liu, and Jiwen Huang. "Research on Permanent Magnet Synchronous Motor Drive System of Electric Vehicle Based on Fuzzy Control." In IOP Conference Series: Earth and Environmental Science, vol. 267, no. 4, p. 042031. IOP Publishing, 2019.

HOW TO CITE THIS ARTICLE

H.Radmanesh, J.Rahmani Fard, Fuzzy Self-tuning PI Controller for Field-weakening Control System of an Axial Flux Switching Permanent Magnet Motor, AUT J. Elec. Eng., 53(2) (2021) 233-248.

DOI: 10.22060/eej.2021.19544.5400